



# Fabrication of highly dense arrays of nanocrystalline diamond nanopillars with integrated silicon-vacancy color centers during the growth

ALEXANDER SCHMIDT,<sup>1</sup> BORIS NAYDENOV,<sup>2,3</sup> FEDOR JELEZKO,<sup>2</sup>  
JOHANN PETER REITHMAIER,<sup>1</sup> AND CYRIL POPOV<sup>1,\*</sup> 

<sup>1</sup>*Institute of Nanostructure Technologies and Analytics, Center for Interdisciplinary Nanostructure Science and Technology, University of Kassel, Heinrich-Plett-Str. 40, D-34132 Kassel, Germany*

<sup>2</sup>*Institute for Quantum Optics, University of Ulm, Albert Einstein Allee 11, D-89081 Ulm, Germany*

<sup>3</sup>*Currently with the Institute for Nanospectroscopy, Helmholtz-Zentrum Berlin für Materialien und Energie GmbH, Berlin, Germany*

\*[popov@ina.uni-kassel.de](mailto:popov@ina.uni-kassel.de)

**Abstract:** Highly dense arrays of diamond nanopillars have been fabricated using nanocrystalline diamond films (NCD) as the starting material. The fabrication process consisted of electron beam lithography (EBL), aluminum mask deposition and inductively coupled O<sub>2</sub> plasma reactive ion etching. The EBL pattern fidelity was enhanced by proximity corrections and dose variations. Optical characterizations of the arrays indicated the incorporation of silicon-vacancy centers during NCD growth as well as enhanced fluorescence and photoluminescence intensities in the well-developed pillar arrays. Transferring this fabrication method to monocrystalline diamond, such dense arrays of diamond nanopillars could be applied in quantum photonics as emitter arrays or photonic crystals upon integration of color centers.

© 2019 Optical Society of America under the terms of the [OSA Open Access Publishing Agreement](#)

## 1. Introduction

Recently, diamond has attracted an ever-increasing interest as a unique platform for quantum information technology (QIT) components and devices like quantum memories, quantum repeaters [1] or single photon sources [2,3] based on the outstanding properties of different color centers in its crystal lattice. One of the most prominent luminescent diamond defects is the nitrogen-vacancy (NV) center, which is composed of a vacancy in the diamond lattice adjacent to a nitrogen atom substituting a carbon atom. Another promising candidate is the silicon-vacancy (SiV) center, composed of a silicon atom between two vacant lattice sites. Such defects are referred to as “artificial atoms” in the solid state, since they exhibit the quantum mechanical properties of single atoms but are embedded in solids that can be processed with modern fabrication techniques [4]. Especially the negatively charged state of NV centers exhibits distinctive electron spin properties which include an easy initialization and manipulation (e.g. with microwaves) and read out [5]. Additionally, the spin decoherence shows long  $T_2$  times, reaching the millisecond range at room temperature [6]. However, the emission spectra of the NV centers reveal a strong phonon-broadening and only a few percent of the photons are emitted in the zero-phonon line (ZPL) [7]. The emission of SiV centers shows a sharp ZPL at 738 nm, a weak phonon side band at room temperature and a very short photoluminescence lifetime of 1–4 ns [8].

To achieve a maximum fluorescence output and collection efficiency of the emitted photons, the color centers should be integrated in photonic structures, serving as optical resonators, e.g., in diamond nanopillars [9–12], photonic crystals [7,13–18], microrings [19], nanobeam photonic crystal cavities [20], microdisks [21], etc. Calculations and measurements have shown that the

fluorescence intensities of NVs in pillars depend on their diameters. Nanopillars with a diameter of ca. 195 nm exhibited a maximum output, which would enhance an optical readout [10].

The creation of NV or SiV centers can be achieved in different ways: i) N or Si ion implantation into diamond, which additionally leads to the formation of vacancies along the implantation tracks. A subsequent annealing enhances the migration of vacancies towards the substitutional implanted ions in the lattice [22–24]. ii) in situ doping by introducing precursor sources into the reaction chamber during the diamond growth. Therefore, precursor gases like SiH<sub>4</sub> or N<sub>2</sub> can be used to create SiV or NV centers, respectively [25–27]. In addition, it has been shown that the formation of NV centers can be achieved in a controlled way with nanometer-precision depth control (delta-doping) [26] or without depth control by a general background level of nitrogen in the reaction chamber [27]. SiV centers can be also created in situ by the presence of a bare silicon source (e.g. a silicon wafer substrate or a piece of crystalline silicon placed close to the substrate) and its etching by atomic hydrogen stemming from the reactant gases during the deposition process [28–29]. In the last years, deterministic single ion implantation methods with nanometer resolution have been demonstrated, which can advance the development of scalable quantum devices based on the integration of color centers (single or ensembles of NV or SiV) into individual diamond nanostructures [30–33].

In this work we study the fabrication of highly dense arrays of nanopillars in nanocrystalline diamond (NCD) films by a “top-down” approach and the optical properties of SiV centers incorporated within the pillars during NCD deposition. Such structures with a periodicity of several hundreds of nanometers, i.e. on the order of the wavelengths of the photons in the visible range, can be applied as photonic crystals. Similar arrays can also be fabricated on NCD membranes, as shown by our recent publication [34]. Another fabrication method was demonstrated by Ondic et al. using a direct “bottom-up” growth on a patterned quartz substrate for creation of 2D photonic crystal slabs to enhance the extraction efficiency of SiV photoluminescence [29]. However, maintaining well-defined cylindrical columns may be difficult using this bottom-up approach.

Upon transferring our fabrication technique to monocrystalline diamond, such arrays can be used as photonic crystals as shown by Cui et al., demonstrating dense nanopillar arrays with a diameter of 168 nm, a period of 230 nm and a L3 defect cavity as hybrid plasmonic photonic crystal cavity structure in monocrystalline diamond to enhance selectively the emission from near-surface NV centers in diamond [14]. One major challenge in the fabrication process was reported regarding substantial proximity effects, despite software corrections during the electron beam lithography (EBL), leading to larger than anticipated feature sizes and therefore mode shifts in the fabricated structures. As for all closely packed nanostructures, such effects and counter-measures will be discussed in the current work for various pillar diameters and periods.

For accurate nanostructuring of NCD material it is necessary to reduce the intrinsic surface roughness of NCD films (from 20–50 nm down to ca. 2 nm) utilizing different planarization processes, which has been demonstrated by several groups [35–37]. In the present study our previous results regarding the fabrication of diamond nanopillars with a large center-to-center (CTC) distance of 5 μm in which SiV centers were incorporated by a short overgrowth [28] and the developed and optimized planarization process of NCD surfaces [37] were exploited as starting points for the preparation of dense arrays of nanopillars with CTC distances more than one order of magnitude smaller, facing additional technological challenges.

## 2. Material and methods

### 2.1. Diamond film deposition

NCD films were deposited in a self-designed hot-filament chemical vapor deposition (HFCVD) setup from a 1% CH<sub>4</sub>/H<sub>2</sub> mixture. Seven tungsten filaments were used to coat three-inch wafers quite homogeneously. More details about the setup can be found in a previous publication [38].

The other major deposition parameters were as follows: Substrate temperature of ca. 890 °C, filament temperature of ca. 2000 °C, and working pressure of 25 mbar. The deposition time was 3 h resulting in ca. 600 nm thick films, which is the height of the pillars to be expected in this study.

As substrates (100) silicon wafers were used, which were pretreated in an ultrasonic bath with a suspension of diamond powders of different sizes in n-pentane to achieve a nucleation density of  $1 \times 10^{10} \text{ cm}^{-2}$  [39]. The resulting NCD films were thoroughly characterized by scanning electron microscopy (SEM), X-ray diffraction, X-ray photoelectron spectroscopy (XPS), Raman spectroscopy with excitation wavelength of 488 nm and secondary ion mass spectrometry (SIMS) applying  $3 \text{ keV Cs}^+$  ( $150 \mu\text{m}^2$ ) for sputtering and  $\text{Bi}_3^{++}$  ( $60 \mu\text{m}^2$ ) for the analysis. They are closed with faceted topography determined by the individual diamond grains with sizes of several hundreds of nanometers as revealed by SEM image in Fig. 1(a).

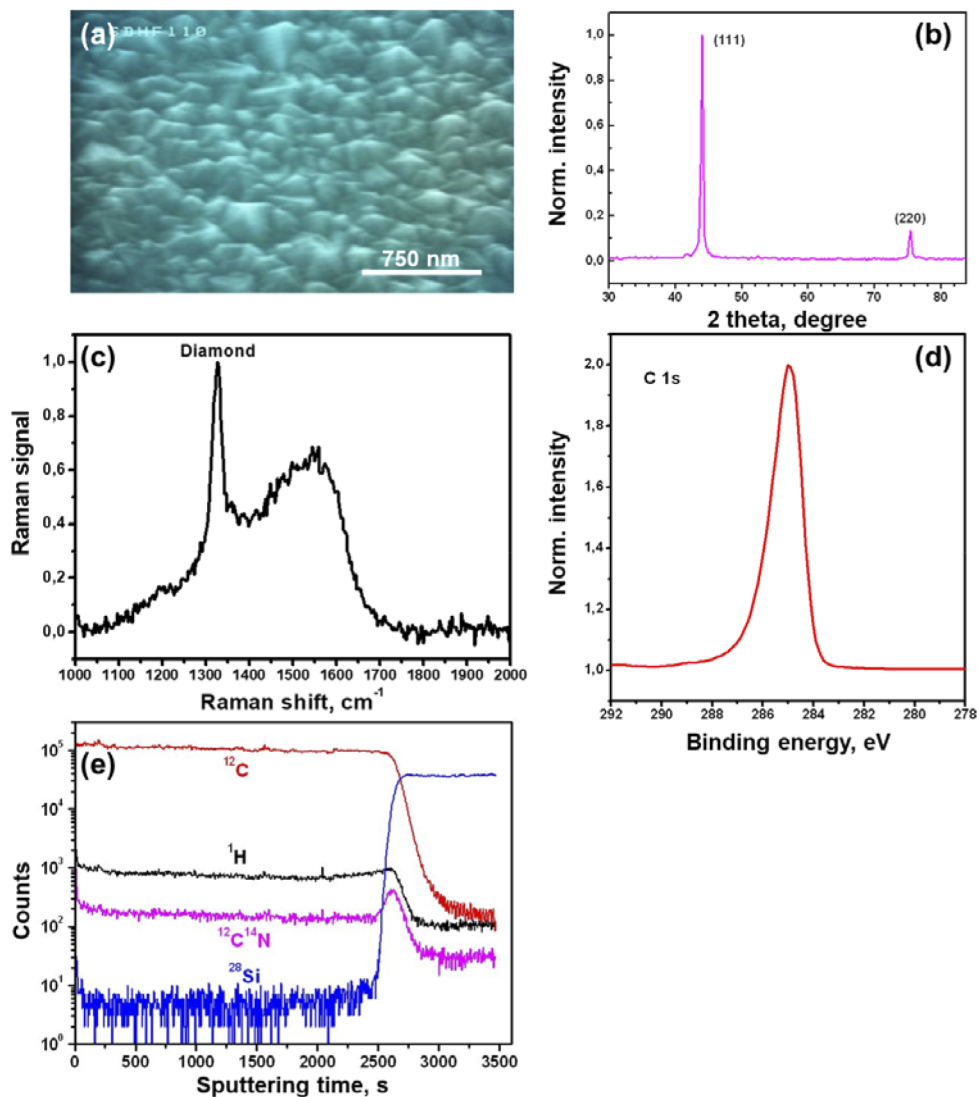


**Fig. 1.** Characterization of the as-grown NCD films: (a) SEM image, (b) XRD pattern, (c) Raman spectrum, (d) XPS C 1s spectrum and (e) SIMS depth profile.

The XRD pattern in Fig. 1(b) taken at grazing incidence angle of  $1^\circ$  showed the (111) and (220) diamond peaks at  $2\theta$  of  $44.0^\circ$  and  $75.4^\circ$ , respectively. The Raman spectrum in Fig. 1(c) exhibited the diamond line at  $1332\text{ cm}^{-1}$  as well as the presence of non-diamond phase in the grain boundary material. Having in mind the lower Raman cross-section for  $\text{sp}^3$  carbon as compared to  $\text{sp}^2$  carbon it can be considered that the diamond phase predominated and the NCD films contained minor amount of non-diamond phase. Having in mind the positions of the X-ray diffractions and of the diamond Raman line it can be considered that there is no stress in the NCD films deposited and structured in the current work. The low  $\text{sp}^2$  carbon content was confirmed by the analysis of the XPS C 1s core spectrum in Fig. 1(d). It revealed a relatively narrow peak which can be attributed to  $\text{sp}^3$  C-C and C-H bonds. There is no distinct broadening at the low energy side where the contribution of  $\text{sp}^2$  C-C should be expected. The tail observed at the high energy side can be assigned to various C-O bonds formed by the contact of the NCD surface with the air. The surface oxygen content was up to 4.3 at% as determined by XPS. The SIMS results (Fig. 1(e)) exhibited homogeneous distribution of N, stemming from the background pressure of  $10^{-3}$  mbar in the chamber and detected as  $\text{CN}^-$  and Si originating from the silicon wafer, in depth of the NCD film with a thickness of ca. 600 nm.

## 2.2. Planarization of the NCD films

Our NCD films were subjected to a planarization process to reduce their inherent surface roughness. Therefore, a spin-on-glass (SOG) (20 wt% perhydropolysilazane (PHPS) in n-dibutylether, NN120-20 from durXtreme) was spin-coated on top of the NCD films, followed by an annealing step at  $180^\circ\text{C}$  for 1 h on a hot plate. Subsequently, they were subjected to an inductively coupled plasma reactive ion etching (ICP RIE) process (Oxford Plasmalab 1000) with the following major process parameters: no ICP power, RF power of 250 W,  $\text{O}_2$  flow of 23 sccm,  $\text{SF}_6$  flow of 2 sccm, working pressure of 5 mTorr, etching duration 8 min and substrate temperature of  $30^\circ\text{C}$ , which was kept constant using a controlled table height and He-backing. The application of the SOG and the etching process was repeated, but for 6 min the second time. Any residual SOG was removed with HF. Following this procedure, the root mean square roughness could be reduced from typical 20-50 nm (of the as-grown samples) to 2-6 nm, for further information about this process please see Ref. [37].

## 2.3. Structuring of the NCD nanopillar arrays

The structuring of the NCD films was performed by EBL and RIE. The lithography started with the spin-coating of a positive resist (AR-P 617.06, Allresist). The desired structures were defined by EBL (Raith eline). They consisted of multiple arrays of dots with three different diameters (200, 100 and 50 nm) and decreasing periods (CTC distances) starting from 400 nm down in 50 nm steps. The exposure doses were varied in a wide range between 10 and  $500\ \mu\text{C}/\text{cm}^2$  in the preliminary tests. The experimental results showed that the best shaped individual pillars and arrays (as a whole) developed in the range of  $40\text{--}70\ \mu\text{C}/\text{cm}^2$  depending on the pillar dimensions and periods. For this reason the applied basic exposure dose was  $42\ \mu\text{C}/\text{cm}^2$  and it was varied with factors in the range between 0.5 and 2. Additionally, proximity corrections were calculated with Raith software "NanoPECS" to reduce the typical overexposure of the center of the arrays.

Subsequently, the resist was developed and a 200 nm layer of aluminum was deposited by electron beam evaporation as a hard mask. A following lift-off process removed the remaining resist together with the aluminum film on top of it. After the lithography step, the patterned NCD samples were subjected to ICP RIE with oxygen (Oxford Plasmalab 1000) to fabricate the pillars. The major process parameters were as follows: ICP power of 1000 W, RF power of 200 W,  $\text{O}_2$  flow of 10 sccm, working pressure of 5 mTorr, and substrate temperature of  $30^\circ\text{C}$ . The typical etch rates with this recipe were around 100 nm/min and endpoints were determined with a laser interferometer (675 nm wavelength). For further information about the etch recipe

and a systematically study of the influence of the process parameters on the etch rates please see Ref. [40]. After the etching process the aluminum mask was removed with a mixture of phosphoric acid, nitric acid and acetic acid ( $\text{H}_3\text{PO}_4:\text{HNO}_3:\text{CH}_3\text{COOH}:\text{H}_2\text{O} = 80\%: 5\%: 5\%: 10\%$ ), followed by cleaning in piranha solution ( $\text{H}_2\text{SO}_4:\text{H}_2\text{O}_2 = 3:1$ ) for 1 min.

#### 2.4. Optical characterization of the pillar arrays

All nanopillar arrays obtained by the processes described above were characterized by means of SEM (Hitachi S-4000) with an acceleration voltage of 10 kV under a tilting angle of  $65^\circ$  or from a  $90^\circ$  topview.

Optical measurements were performed on a home built confocal microscope controlled by the Qudi software suite [41]. The excitation was achieved with a laser with a wavelength of 518 nm (Toptica iBeam smart) and excitation power of  $100 \mu\text{W}$ , the fluorescence was detected through a 640 nm long pass filter by two APDs (Excellitas). The photoluminescence spectra were taken with a spectrometer (Princeton Instruments, IsoPlane 160, CCD PIXIS 100B).

### 3. Results and discussion

#### 3.1. Characterization of the pillar arrays

Arrays of NCD nanopillars with nominal diameters of 200, 100 and 50 nm were fabricated as described in section 2. Their defined period (CTC distance) was decreased in steps of 50 nm starting from 400 nm. The resulting nanopillars were larger than defined by EBL and this effect increased with decreasing the nominal diameter of the pillars as can be seen in Fig. 2 and Table 1.

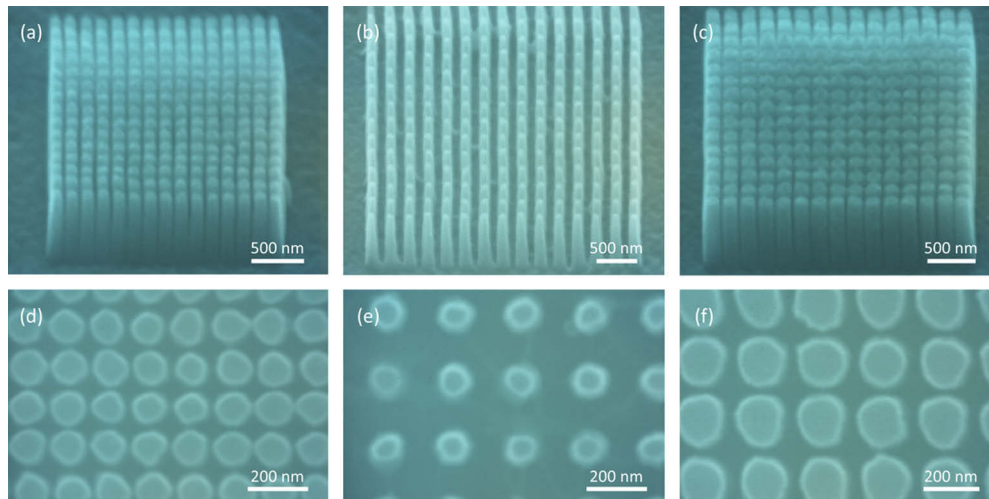


**Fig. 2.** SEM images of NCD pillar arrays with nominal diameters of 50 nm (a, b) and 100 nm (c) with a period of 150 nm (a), 250 nm (b) and 200 nm (c). The first row (a-c) shows an overview of the whole array from a  $65^\circ$  angle, whereas the second row (d-f) shows a magnification of the center of the array from a topview.

In the case of the 50 nm defined pillars the measured diameters were  $(117 \pm 7)$  nm and  $(111 \pm 7)$  nm for nominal periods of 150 nm and 250 nm, respectively. At the same time the measured pitches (spacings between the sidewalls of the pillars to their next neighbors) were considerably smaller. An overview for comparison between the nominal defined and measured values of the nanopillar diameters and pitches is presented in Table 1. For each diameter two values are given, the first one from the arrays with the closest resolved structures and the second one from arrays

**Table 1. Overview of the nominal written and measured dimensions of the NCD nanopillar arrays.**

nominal	Ø (nm)		pitches between the pillars (nm)	
	measured	period	nominal	measured
50	117 ± 7	150	100	35 ± 7
50	111 ± 7	250	200	132 ± 7
100	160 ± 6	200	100	43 ± 9
100	178 ± 6	300	200	114 ± 9
200	207 ± 5	300	100	90 ± 6
200	208 ± 5	350	150	135 ± 6

with a considerably larger period (CTC distance). All values were estimated from SEM topview images.

The enlargement of the pillar diameters (in case of 50 and 100 nm) could be attributed to proximity effects in EBL despite software corrections. The exposure resolution is affected by electron–solid interactions and thus inherent electron scattering phenomena. The latter occur as the electrons penetrate through the resist into the substrate and lead to an undesired exposure in the regions adjacent to those addressed by the electron beam. Proximity corrections were calculated with “NanoPECS” software by adjusting the incident electron exposure dose of each pillar of the array. In addition, the exposure dose was varied as mentioned in section 2. A typical result with and without proximity corrections and dose adjustments can be seen in Fig. 3(a, b). The center of the array was completely unresolved, due to a strong enlargement of the pillars and their merge together. An exemplary calculated exposure dose distribution from the proximity correction software is shown in Fig. 3(c).

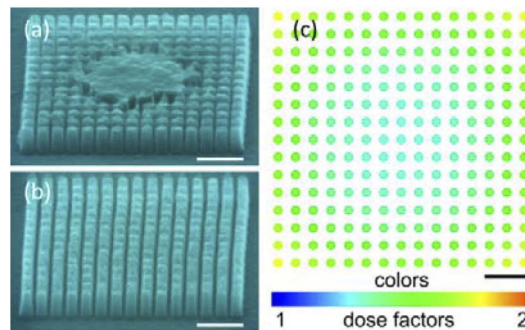


**Fig. 3.** Typical SEM micrographs depicting the merge of the nanopillars in the center of the array without proximity corrections (a) and with corrective means (b). Exemplary overview of the relative electron dose distribution within the array from the proximity correction software (c). Scale bars indicate 1  $\mu\text{m}$ . For colors please see online version.

The defined 50 nm pillar arrays with nominal pitches of 100 nm and 200 nm were best resolved with exposure doses in the EBL step of 58.8  $\mu\text{C}/\text{cm}^2$  and 63  $\mu\text{C}/\text{cm}^2$ , respectively. It has to be noted that already small deviations of the exposure dose of ca.  $\pm 5 \mu\text{C}/\text{cm}^2$  led to severely deteriorated arrays, where either pillars were missing due to underdevelopment or were enlarged and merged together. The optimal value also differed for each pattern design and therefore an exposure dose variation was also crucial to obtain the best resolved structures in addition to proximity corrections.

A closer observation of the topview SEM images revealed that the shape of the pillars was slightly deformed and not perfectly round. This can be attributed to the following effects: (i)

charging effects in the EBL step, typically deforming the desired structures, especially since our material of interest NCD is not conductive; (ii) proximity effects in EBL, since the pillar diameters are still enlarged; (iii) the surface roughness, which complicates the overall structuring process and for this reason we already use a planarization process for our NCD films (see section 2.2); (iv) a mask erosion during the ICP RIE step. Figure 4 shows typical hard masks for structuring of arrays of pillars with nominal diameters of 50 nm and two different periods. As seen from this figure the shapes of the masks are already not perfectly round which can be at least partially due to the remaining surface roughness of the NCD after planarization. This roughness could contribute also to the scattering of photons emitted from the incorporated color centers.

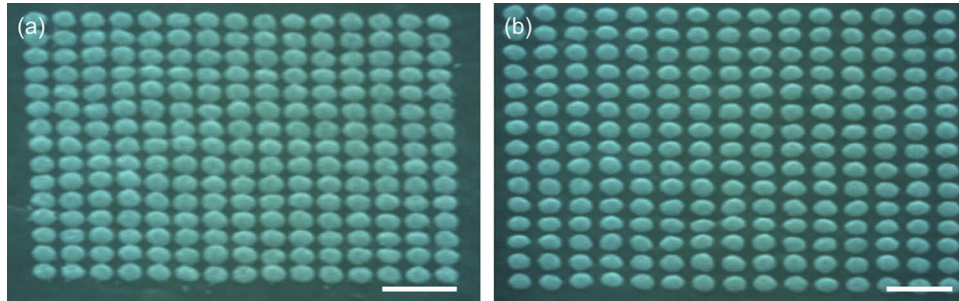


**Fig. 4.** Exemplary SEM micrographs of typical hard mask shapes before reactive ion etching: (a) an array for pillars with nominal diameters of 50 nm and a period of 200 nm, (b) an array for pillars with nominal diameters of 50 nm and a period of 250 nm. Scale bars indicate 500 nm.

The sidewalls of the pillars are vertical. Only their upper part was slightly tapered, but to a much lesser degree than in previous works, where we fabricated single nanopillars separated by multiple microns [27]. There the pillar top diameters were significantly smaller than the bottom diameters compared to equal NCD pillar dimensions in the current study. One reason could be the lack of overetching in the RIE step: the closer package of the pillars in this study limits the overall exposure of the individual pillars to the plasma in comparison to the ones with a much larger period. It can be assumed that our standard etching recipe (see section 2.3) utilizes a combination of both chemical and physical etching. Especially the physical sputter component could be influenced by a closer package of the pillars, if the lateral distances between the pillars reach magnitudes of the mean free path of the impinging ions from the plasma. Another observation can underline this aspect: The nanopillars at the very rim of an array were in general slightly stronger etched and therefore a bit more tapered than the pillars inside the array.

In general, similar results were obtained regarding the influence of the pitches between the pillars with nominal diameters of 100 nm (see Fig. 2) and 200 nm (see Table 1) except that in the latter case the diameters were close to the defined dimensions ( $207 \pm 5$ ) nm. In the case of 200 nm pillars, the best structures were obtained for an exposure dose of  $50 \mu\text{C}/\text{cm}^2$  for a period of 300 nm, and  $46 \mu\text{C}/\text{cm}^2$  for a period of 350 nm, respectively. For the 100 nm pillars the following values were measured: ( $160 \pm 6$ ) nm in the case of 200 nm period with an optimal exposure dose of  $71 \mu\text{C}/\text{cm}^2$  and ( $178 \pm 6$ ) nm for 300 nm period with an optimal exposure dose of  $51 \mu\text{C}/\text{cm}^2$ .

Further optimizations of the fabrication process are still possible to achieve a higher fidelity of the pattern design. For example, the exposure dose variation could include even smaller steps. In addition to proximity corrections, the feature sizes in the pattern design could be decreased, so that the resulting structures will match the specified dimensions including the enlargement while structuring in the EBL.

### 3.2. Optical properties of the pillars

The optical properties of the fabricated arrays of dense NCD nanopillars were investigated by fluorescence mapping and photoluminescence (PL) spectroscopy. Different pillar arrays, including such prepared without proximity corrections and dose adjustments, i.e. with unresolved center of the array as shown in Fig. 3(a), were investigated with a confocal microscope; typical fluorescence maps are presented in Fig. 5. The fluorescence maps of the fully developed arrays demonstrated large bright spots due to the overlapped signals of all pillars in the array resulting from the small period. The average fluorescence intensities of the array spots ( $7\text{--}8 \times 10^6$  cps) were on the same order of magnitude as of pillars with a diameter of 200 nm but with a larger period of 5  $\mu\text{m}$ , which were fabricated from NCD deposited using the same deposition system and parameters, structured under the same conditions and measured with a similar set-up [27]. The intensity at the rim of the arrays was higher (reaching in some cases ca.  $12 \times 10^6$  cps (Fig. 5(a)) which can be attributed to the slightly different shape (more tapered) of the pillars at the rim of the array, as mentioned above. In the case of not completely resolved arrays, the “bulk” part in the center showed fluorescence with much lower intensity compared to the part with structured nanopillars (Fig. 5(b)), which might be related to enhanced photon collection efficiency in the latter case.

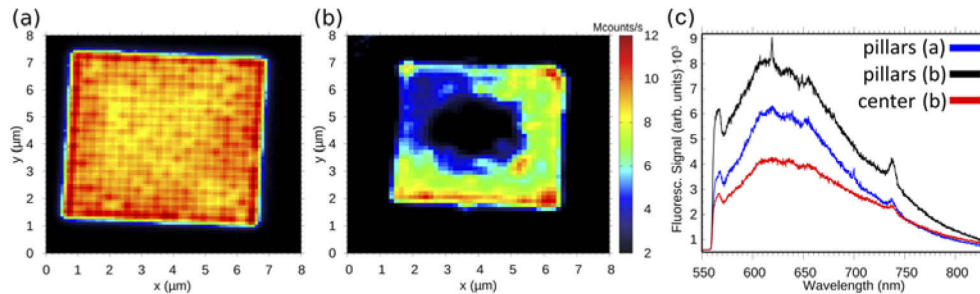


**Fig. 5.** Confocal images showing the fluorescence of an array of 200 nm pillars and a period of 400 nm with completely resolved diamond nanopillars after proximity correction (a) and with unstructured center without proximity correction (b), and the corresponding room temperature PL spectra (c) of the arrays of diamond nanopillars.

Typical room temperature photoluminescence spectra of NCD pillar arrays are shown in Fig. 5(c). The PL spectra indicate the presence of silicon-vacancy (SiV) color centers with a ZPL at 738 nm in the nanopillars. Although the peaks of  $\text{NV}^0$  and  $\text{NV}^-$  with ZPLs at 575 and 637 nm, respectively, were not observed in the PL spectra, their presence having in mind the nitrogen content in the grown NCD films could not be excluded being completely overlapped by a broad phonon sideband. NV centers can be incorporated in the CVD diamond relying on the nitrogen background level, even if the proportion of N atoms from the gas phase that form NV centers in the grown diamond is low ( $5 \times 10^{-8}$ ) [42]. The incorporation of Si in the NCD appeared during the growth with atoms etched from the silicon substrate by the atomic hydrogen from the gas phase before being completely coated. The ZPL of SiVs is overlapped by the broad band which is typical for poly- and nanocrystalline CVD diamond. The intensity of the signal taken from areas with structured pillars was higher than that from the “bulk” unstructured center of arrays prepared without proximity correction most probably due to the enhanced photon collection. Fluorescence images of arrays with higher package density or smaller pillar diameters showed only one bright square without noticeable individual bright spots, reaching the resolution limit of the confocal microscope.

#### 4. Conclusions

We have shown the fabrication of highly dense arrays of nanopillars from nanocrystalline diamond films with nominal diameters of 200, 100 and 50 nm by means of EBL and ICP RIE with oxygen plasma. The main fabrication step (EBL) was enhanced with proximity corrections and exposure dose variations. Well-resolved nanopillars with various diameters and periods were prepared. The pillars with diameters below 200 nm were enlarged compared to the nominally defined values despite the proximity corrections. Pitches between the pillar sidewalls down to 35 nm were achieved. Further improvements of the resulting sizes of the pillars compared to the nominal values could be obtained by even finer adjustments of the EBL parameters and reduced feature sizes in the EBL pattern.

Optical characterizations of the structured nanopillars indicated the presence of SiV centers incorporated in situ during the NCD growth. The fluorescence intensities were enhanced by well-developed pillar arrays with proximity corrections compared to pillar arrays with merged centers without any corrective means. Transferring this fabrication process to monocrystalline diamond, such highly dense nanopillar arrays with incorporated color centers (SiVs or NVs) could be a promising platform for optical cavities, dense emitter arrays or photonic crystals.

#### Funding

Volkswagen Foundation, project “Quantum coins and nanosensors” (Az. 91001).

#### Disclosures

The authors declare no conflicts of interest.

#### References

1. A. A. Bukach and S. Y. Kilin, “Quantum repeater based on NV +  $^{13}\text{C}$  color centers in diamond,” *Opt. Spectrosc.* **103**(2), 202–209 (2007).
2. C.-H. Su, A. D. Greentree, and L. C. L. Hollenberg, “High-performance diamond-based single-photon sources for quantum communication,” *Phys. Rev. A* **80**(5), 052308 (2009).
3. I. Aharonovich, S. Castelletto, D. A. Simpson, C.-H. Su, A. D. Greentree, and S. Praver, “Diamond-based single-photon emitters,” *Rep. Prog. Phys.* **74**(7), 076501 (2011).
4. V. Acosta and P. Hemmer, “Nitrogen-vacancy centers: Physics and applications,” *MRS Bull.* **38**(2), 127–130 (2013).
5. M. V. Dutt, L. Childress, L. Jiang, E. Togan, J. Maze, F. Jelezko, A. S. Zibrov, P. R. Hemmer, and M. D. Lukin, “Quantum Register Based on Individual Electronic and Nuclear Spin Qubits in Diamond,” *Science* **316**(5829), 1312–1316 (2007).
6. G. Balasubramanian, P. Neumann, D. Twitchen, M. Markham, R. Kolesov, N. Mizuochi, J. Isoya, J. Achard, J. Beck, J. Tissler, V. Jacques, P. R. Hemmer, F. Jelezko, and J. Wrachtrup, “Ultralong spin coherence time in isotopically engineered diamond,” *Nat. Mater.* **8**(5), 383–387 (2009).
7. A. Faraon, C. Santori, Z. Huang, V. M. Acosta, and R. G. Beausoleil, “Coupling of Nitrogen-Vacancy Centers to Photonic Crystal Cavities in Monocrystalline Diamond,” *Phys. Rev. Lett.* **109**(3), 033604 (2012).
8. H. Sternschulte, K. Thonke, R. Sauer, P. C. Münzinger, and P. Michler, “1.681-eV luminescence center in chemical-vapor-deposited homoepitaxial diamond films,” *Phys. Rev. B* **50**(19), 14554–14560 (1994).
9. B. J. M. Hausmann, M. Khan, Y. Zhang, T. M. Babinec, K. Martinick, M. McCutcheon, P. R. Hemmer, and M. Loncar, “Fabrication of diamond nanowires for quantum information processing applications,” *Diamond Relat. Mater.* **19**(5-6), 621–629 (2010).
10. C. J. Widmann, C. Giese, M. Wolfer, D. Brink, N. Heidrich, and C. E. Nebel, “Fabrication and characterization of single crystalline diamond nanopillars with NV-centers,” *Diamond Relat. Mater.* **54**, 2–8 (2015).
11. A. E. Rugar, C. Dory, S. Sun, and J. Vuckovic, “Characterization of optical and spin properties of single tin-vacancy centers in diamond nanopillars,” *Phys. Rev. B* **99**(20), 205417 (2019).
12. J. L. Zhang, K. G. Lagoudakis, Y.-K. Tzeng, C. Dory, M. Radulaski, Y. Kelaita, K. A. Fischer, S. Sun, Z.-X. Shen, N. A. Melosh, S. Chu, and J. Vuckovic, “Complete coherent control of silicon vacancies in diamond nanopillars containing single defect centers,” *Optica* **4**(11), 1317–1321 (2017).
13. J. Riedrich-Möller, L. Kipfstuhl, C. Hepp, E. Neu, C. Pauly, F. Mücklich, A. Baur, M. Wandt, S. Wolff, M. Fischer, S. Gsell, M. Schreck, and C. Becher, “One- and two-dimensional photonic crystal microcavities in single crystal diamond,” *Nat. Nanotechnol.* **7**(1), 69–74 (2012).

14. S. Cui, X. Zhang, T. Liu, J. Lee, D. Bracher, K. Ohno, D. Awschalom, and E. L. Hu, "Hybrid Plasmonic Photonic Crystal Cavity for Enhancing Emission from near-Surface Nitrogen Vacancy Centers in Diamond," *ACS Photonics* **2**(4), 465–469 (2015).
15. C. F. Wang, R. Hanson, D. D. Awschalom, E. L. Hu, T. Feygelson, J. Yang, and J. E. Butler, "Fabrication and characterization of two-dimensional photonic crystal microcavities in nanocrystalline diamond," *Appl. Phys. Lett.* **91**(20), 201112 (2007).
16. I. Bayn, B. Meyler, A. Lahav, J. Salzman, R. Kalish, B. A. Fairchild, S. Praver, M. Barth, O. Benson, T. Wolf, P. Siyushev, F. Jelezko, and J. Wrachtrup, "Processing of photonic crystal nanocavity for quantum information in diamond," *Diamond Relat. Mater.* **20**(7), 937–943 (2011).
17. T. Schröder, M. Walsh, J. Zheng, S. Mouradian, L. Li, G. Malladi, H. Bakhru, M. Lu, A. Stein, M. Heuck, and D. Englund, "Scalable fabrication of coupled NV center - photonic crystal cavity systems by self-aligned N ion implantation," *Opt. Mater. Express* **7**(5), 1514–1524 (2017).
18. N. H. Wan, S. Mouradian, and D. Englund, "Two-dimensional photonic crystal slab nanocavities on bulk single-crystal diamond," *Appl. Phys. Lett.* **112**(14), 141102 (2018).
19. A. Faraon, P. E. Barclay, C. Santori, K. M. C. Fu, and R. G. Beausoleil, "Resonant enhancement of the zero-phonon emission from a colour centre in a diamond cavity," *Nat. Photonics* **5**(5), 301–305 (2011).
20. J. L. Zhang, S. Sun, M. J. Burek, C. Dory, Y.-K. Tzeng, K. A. Fischer, Y. Kelaita, K. G. Lagoudakis, M. Radulaski, Z.-X. Shen, N. A. Melosh, S. Chu, M. Loncar, and J. Vuckovic, "Strongly Cavity-Enhanced Spontaneous Emission from Silicon-Vacancy Centers in Diamond," *Nano Lett.* **18**(2), 1360–1365 (2018).
21. B. Khanaliloo, M. Mitchell, A. C. Hryciw, and P. E. Barclay, "High-Q/V Monolithic Diamond Microdisks Fabricated with Quasi-isotropic Etching," *Nano Lett.* **15**(8), 5131–5136 (2015).
22. I. Aharonovich, C. Santori, B. A. Fairchild, J. Orwa, K. Ganesan, K.-M. C. Fu, R. G. Beausoleil, A. D. Greentree, and S. Praver, "Producing optimized ensembles of nitrogen-vacancy color centers for quantum information applications," *J. Appl. Phys.* **106**(12), 124904 (2009).
23. B. Naydenov, V. Richter, J. Beck, M. Steiner, P. Neumann, G. Balasubramanian, J. Achard, F. Jelezko, J. Wrachtrup, and R. Kalish, "Enhanced generation of single optically active spins in diamond by ion implantation," *Appl. Phys. Lett.* **96**(16), 163108 (2010).
24. R. E. Evans, A. Sipahigil, D. D. Sukachev, A. S. Zibrov, and M. D. Lukin, "Narrow-Linewidth Homogeneous Optical Emitters in Diamond Nanostructures via Silicon Ion Implantation," *Phys. Rev. Appl.* **5**(4), 044010 (2016).
25. V. Sedov, V. Ralchenko, A. A. Khomich, I. Vlasov, A. Vul, S. Savin, A. Goryachev, and V. Konov, "Si-doped nano- and microcrystalline diamond films with controlled bright photoluminescence of silicon-vacancy color centers," *Diamond Relat. Mater.* **56**, 23–28 (2015).
26. K. Ohno, F. J. Heremans, L. C. Bassett, B. A. Myers, D. M. Toyli, A. C. Bleszynski Jayich, C. J. Palmstrom, and D. D. Awschalom, "Engineering shallow spins in diamond with nitrogen delta-doping," *Appl. Phys. Lett.* **101**(8), 082413 (2012).
27. E. Petkov, T. Rendler, C. Petkov, F. Schnabel, J. P. Reithmaier, J. Wrachtrup, C. Popov, and W. Kulisch, "Investigation of NV centers in nano- and ultrananocrystalline diamond pillars," *Phys. Status Solidi A* **210**(10), 2066–2073 (2013).
28. N. Felgen, B. Naydenov, S. Turner, F. Jelezko, J. P. Reithmaier, and C. Popov, "Incorporation and study of SiV centers in diamond nanopillars," *Diamond Relat. Mater.* **64**, 64–69 (2016).
29. L. Ondic, M. Varga, K. Hruska, J. Fait, and P. Kapusta, "Enhanced Extraction of Silicon-Vacancy Centers Light Emission Using Bottom-Up Engineered Polycrystalline Diamond Photonic Crystal Slabs," *ACS Nano* **11**(3), 2972–2981 (2017).
30. J. Meijer, T. Vogel, B. Burchard, I. W. Rangelow, L. Bischoff, J. Wrachtrup, M. Domhan, F. Jelezko, W. Schnitzler, S. A. Schulz, K. Singer, and F. Schmidt-Kaler, "Concept of deterministic single ion doping with sub-nm spatial resolution," *Appl. Phys. A* **83**(2), 321–327 (2006).
31. J. L. Pacheco, M. Singh, D. L. Perry, J. R. Wendt, G. Ten Eyck, R. P. Manginell, T. Pluym, D. R. Luhman, M. P. Lilly, M. S. Carroll, and E. Bielejec, "Ion implantation for deterministic single atom devices," *Rev. Sci. Instrum.* **88**(12), 123301 (2017).
32. G. Jacob, K. Groot-Berning, S. Wolf, S. Ulm, L. Couturier, U. G. Poschinger, F. Schmidt-Kaler, and K. Singer, "Single particle microscopy with nanometer resolution," arXiv:1405.6480 [physics.atom-ph] (2014).
33. K. Groot-Berning, T. Kornher, G. Jacob, F. Stopp, S. T. Dawkins, R. Kolesov, J. Wrachtrup, K. Singer, and F. Schmidt-Kaler, "Deterministic single ion implantation of rare-earth ions for nanometer resolution colour center generation," arXiv:1902.05308 [quant-ph] (2019).
34. A. Schmidt, J. Bernardoff, K. Singer, J. P. Reithmaier, and C. Popov, "Fabrication of Nanopillars on Nanocrystalline Diamond Membranes for the Incorporation of Color Centers," *Phys. Status Solidi A* 1900233 (2019).
35. M. Rabarot, J. Widiez, S. Saada, J.-P. Mazellier, C. Lecouvey, J.-C. Roussin, J. Dechamp, P. Bergonzo, F. Andrieu, O. Faynot, S. Deleonibus, L. Clavelier, and J. P. Roger, "Silicon-On-Diamond layer integration by wafer bonding technology," *Diamond Relat. Mater.* **19**(7-9), 796–805 (2010).
36. X. Checoury, D. Néel, P. Boucaud, C. Gesset, H. Girard, S. Saada, and P. Bergonzo, "Nanocrystalline diamond photonics platform with high quality factor photonic crystal cavities," *Appl. Phys. Lett.* **101**(17), 171115 (2012).
37. J. Heupel, N. Felgen, R. Merz, M. Kopnarski, J. P. Reithmaier, and C. Popov, "Development of a Planarization Process for the Fabrication of Nanocrystalline Diamond Based Photonic Structures," *Phys. Status Solidi A* **2019**, 1900314 (2019).

38. W. Kulisch, C. Petkov, E. Petkov, C. Popov, P. N. Gibson, M. Veres, R. Merz, B. Merz, and J. P. Reithmaier, "Low temperature growth of nanocrystalline and ultrananocrystalline diamond films: A comparison," *Phys. Status Solidi A* **209**(9), 1664–1674 (2012).
39. W. Kulisch, C. Popov, T. Sasaki, L. Sirghi, H. Rauscher, F. Rossi, and J. P. Reithmaier, "On the development of the morphology of ultrananocrystalline diamond films," *Phys. Status Solidi A* **208**(1), 70–80 (2011).
40. J. Evtimova, W. Kulisch, C. Petkov, E. Petkov, F. Schnabel, J. P. Reithmaier, and C. Popov, "Reactive ion etching of nanocrystalline diamond for the fabrication of one-dimensional nanopillars," *Diamond Relat. Mater.* **36**, 58–63 (2013).
41. J. M. Binder, A. Stark, N. Tomek, J. Scheuer, F. Frank, K. D. Jahnke, C. Müller, S. Schmitt, M. H. Metsch, T. Unden, T. Gehring, A. Huck, U. L. Andersen, L. J. Rogers, and F. Jelezko, "Qudi: A modular python suite for experiment control and data processing," *SoftwareX* **6**, 85–90 (2017).
42. J. R. Rabeau, A. Stacey, A. Rabeau, S. Praver, F. Jelezko, I. Mirza, and J. Wrachtrup, "Single nitrogen vacancy centers in chemical vapor deposited diamond nanocrystals," *Nano Lett.* **7**(11), 3433–3437 (2007).